Molecular Pharmacology Fast Forward. Published on August 27, 2015 as DOI: 10.1124/mol.115.099747
This article has not been copyedited and formatted. The final version may differ from this version.

Structural asymmetry of phosphodiesterase-9A and a unique pocket for selective binding of a potent enantiomeric inhibitor

Manna Huang#, Yong-xian Shao#, Jianying Hou, Wenjun Cui, Beibei Liang, Yingchun Huang, Zhe Li, Yinuo Wu, Xinhai Zhu, Peiqing Liu, Yiqian Wan, Hengming Ke, and Hai-Bin Luo

School of Chemistry and Chemical Engineering (M.H., J.H., X.Z. Y.W.) Sun Yat-Sen University, Guangzhou 510275, PR China

School of Pharmaceutical Sciences (Y.S., Z.L, Y.W., P.L, H-B.L), Sun Yat-Sen University, Guangzhou 510006, PR China

Department of Biochemistry and Biophysics and Lineberger Comprehensive Cancer Center (W.C, B.L, Y.H, H.K) , The University of North Carolina, Chapel Hill, NC 27599-7260, USA

Molecular Pharmacology Fast Forward. Published on August 27, 2015 as DOI: 10.1124/mol.115.099747
This article has not been copyedited and formatted. The final version may differ from this version.

Running Title: Asymmetric recognition of PDE9 inhibitors

Address correspondence to:

Dr. Hengming Ke, the University of North Carolina, 120 Mason Farm Road, Chapel Hill, NC 27599, Tel: 1-919-966-2244, email: hke@med.unc.edu, or Dr. Hai-Bin Luo, School of Pharmaceutical Sciences, Sun Yat-Sen University, Guangzhou 510006, PR China, Tel: 86-20-39943031, email: luohb77@mail.sysu.edu.cn, or Dr. Yiqian Wan, School of Chemistry and Chemical Engineering Sun Yat-Sen University, Guangzhou 510275, PR China, Tel: 86-20-84113610, email: ceswyq@mail.sysu.edu.cn.

The number of text pages: 19

The number of tables: 6

The number of figures: 5

The number of references: 42

The number of words in the *Abstract*: 148

The number of words in *Introduction*: 418

The number of words in *Discussion*: 386

Abbreviations

PDE, phosphodiesterase; cGMP, cyclic guanosine monophosphate; cAMP, cyclic adenosine monophosphate; IBMX, 3-isobutyl-1-methylxanthine; TLC, thin layer chromatography.

Molecular Pharmacology Fast Forward. Published on August 27, 2015 as DOI: 10.1124/mol.115.099747
This article has not been copyedited and formatted. The final version may differ from this version.

ABSTRACT

Phosphodiesterase-9 (PDE9) inhibitors have been studied as potential therapeutics for treatment of CNS diseases and diabetes. Here we report discovery of a new category of PDE9 inhibitors by rational design on the basis of the crystal structures. The best compound (S)-**C33** has IC_{50} of 11 nM against PDE9 and the racemic **C33** has bioavailability of 56.5% in the rat pharmacokinetic model. The crystal structures of PDE9 in complex with racemic **C33**, (R)-**C33**, and (S)-**C33** reveal subtle conformational asymmetry of two M-loops in the PDE9 dimer and different conformations of two **C33** enantiomers. The structures also identified a small hydrophobic pocket that interacts with the tyrosyl tail of (S)-**C33** but not (R)-**C33** and is thus possibly useful for improvement of selectivity of PDE9 inhibitors. The asymmetry of the M-loop and different interactions of **C33** enantiomers imply a necessity of consideration of the whole PDE9 dimer for design of inhibitors.

Molecular Pharmacology Fast Forward. Published on August 27, 2015 as DOI: 10.1124/mol.115.099747
This article has not been copyedited and formatted. The final version may differ from this version.

INTRODUCTION

Phosphodiesterase (PDE) is a superfamily of enzymes hydrolyzing second messengers cGMP and cAMP. For the critical roles of cAMP and cGMP in physiological processes, PDEs have been studied as drug targets for treatment of various diseases (Conti and Beavo, 2007; Maurice et al., 2014). Human genome contains 21 genes that are categorized into 11 PDE families and express >100 isoforms (Conti and Beavo, 2007; Maurice et al., 2014). PDE5, PDE6, and PDE9 specifically recognize cGMP as their substrate, while PDE4, PDE7, and PDE8 are cAMP-specific. The remaining PDE families are capable of degrading both substrates. PDE9 inhibitors have been studied for their potential applications to treat diabetes (Deninno et al., 2009; Shao et al., 2014) and CNS diseases such as Alzheimer's disease (Wunder et al., 2005; van der Staay et al., 2008; Hutson et al., 2011; Vardigan et al., 2011; Verhoest et al., 2009; 2012; Claffey et al., 2012; Kleiman et al., 2012; Kroker et al., 2012; Liddie et al., 2012; Kroker et al., 2014; Schwam et al., 2014; Singh et al., 2014; Heckman et al., 2015; Nagy et al., 2015).

On the other hand, since almost all important bio-macromolecules such as proteins and nucleic acids exist in chiral forms, enantiomeric molecular recognition is the most important biological process in nature. Similarly, when exogenous compounds such as drugs are introduced into the human body, chiral discrimination plays a fundamental role in determining pharmacokinetic properties and bio-recognition of drugs in physiological processes (Agranat et al., 2002). The market share for single-enantiomer drugs increases from 27% (US$74.4 billion) in 1996 to 40-50% in the pharmaceutical market today (Shaner et al., 2005; Sekhon, 2013). Recently, legal regulation intends to allow only single-enantiomer drugs to be marketed (Mentel et al., 2009). In spite of importance of the drug chirality, the impacts of potentially different binding of enantiomers on biological effects have not been completely illustrated (Londesborough, 1985).

Molecular Pharmacology Fast Forward. Published on August 27, 2015 as DOI: 10.1124/mol.115.099747
This article has not been copyedited and formatted. The final version may differ from this version.

In this paper, we report a novel category of PDE9 inhibitors that are discovered by the rational structure-based design and docking on the basis of our early analogs of **28s** and **3r** (Meng et al., 2012; Shao et al., 2014). Crystal structures of PDE9 in complex with the best compound, (S)-**C33**, and a systematic comparison among PDE9 structures in the RCSB Protein Data Bank revealed subtle but significant conformation difference between two M-loops in PDE9 dimers. In addition, the crystal structure of PDE9A-**C33** identified a small hydrophobic pocket that interacted with (S)-**C33** only and may thus play a critical role in determination of inhibitor selectivity.

Materials and methods

Molecular docking

PDE9A (PDB ID: 4GH6) was used for docking by CDOCKE (Wu et al., 2003) and Ligandfit (Venkatachalam et al., 2003) embedded in Accelrys Discovery Studio 2.5.5. Hydrogen atoms and charges were generated by the CHARMM force field and the Momany-Rone partial charge method. All ionizable residues were set to their protonation states. Charges of zinc and magnesium ions were assigned to +2. The radius of docking sphere was set to 10 Å. The default values were used for rest docking parameters. The PDE9A inhibitor **28s** (Meng et al., 2012) was used as a reference for test of docking. The reliability of the docking results is also confirmed by the comparison between the docking poses and the crystal structure of PDE9-(S)-C33 (supplemental information S1). Fifty conformations of each ligand were randomly generated, docked and output for evaluation. The candidates with high scores and reasonable binding patterns were chemically synthesized.

Molecular Pharmacology Fast Forward. Published on August 27, 2015 as DOI: 10.1124/mol.115.099747
This article has not been copyedited and formatted. The final version may differ from this version.

Synthesis

^{1}H NMR and ^{13}C NMR spectra were recorded at room temperature on a Bruker AVANCE III 400 instrument with TMS as an internal reference. LC/MS equipment LCMS-2010A was used for mass analysis. Thin-layer chromatography (TLC) was performed on precoated silica gel F-254 plates (0.25 mm, E. Merck). Elemental analysis was carried out with a Vario EL series analyzer. Melting points were determined on a WRS-1B digital melting point apparatus and were not calibrated. IR spectra were recorded on a Thermo 330 FT-IR. All starting materials and reagents were purchased from commercial suppliers and used directly without further purification. The syntheses of the compounds are outlined in scheme 1.

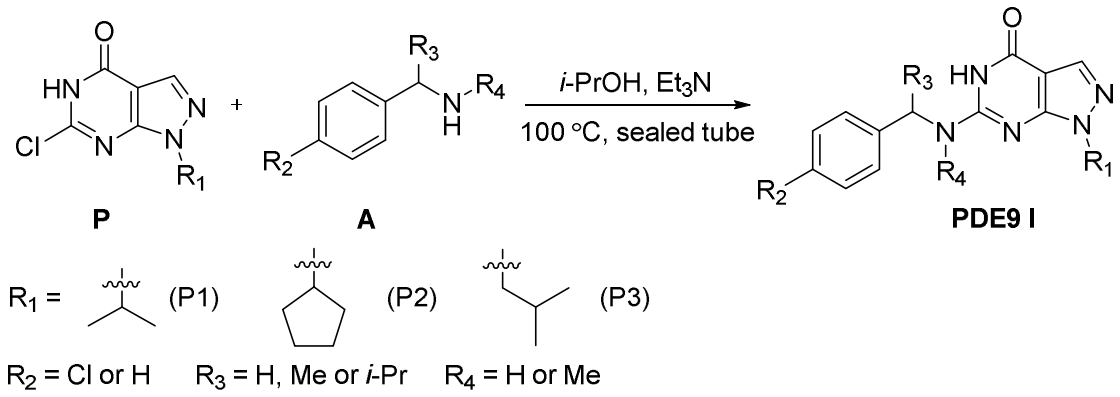

Scheme 1. Synthesis of PDE9 inhibitors (**PDE9 I**)

Compounds **P1-P3** were synthesized according to the protocol previously reported (Shao et al., 2014). The syntheses of the target compounds are briefly described as follows. To a 10 mL sealed vial were added *i*-PrOH (2 mL), pyrimidinone (**P**, 0.3 mmol), amine (**A**, 1.0 mmol), and Et_3N (1.0 mmol). The reaction mixture was stirred in an oil bath preheated to 100 ºC. After **P** was consumed as indicated by TLC, the reaction mixture was cooled to room temperature and concentrated in vacuo. The residue was purified by flash column chromatography on silica gel to provide the target compounds. The following are characterizations of the targeted compounds.

Molecular Pharmacology Fast Forward. Published on August 27, 2015 as DOI: 10.1124/mol.115.099747
This article has not been copyedited and formatted. The final version may differ from this version.

*(±)-1-isopropyl-6-((1-phenylethyl)amino)-1,5-dihydro-4H-pyrazolo[3,4-d]pyrimidin-4-one (**H10**).* white solids (83 mg, yield: 93%). M.p.: 67-68 ºC; MS (ESI$^-$): *m/z*: 296 ([M-H]$^-$); ^{1}H NMR (400 MHz, $CDCl_3$) 10.70 (brs, 1H), 7.59 (s, 1H), 7.47 - 7.42 (m, 2 H), 7.35 (t, *J* = 7.5 Hz, 2 H), 7.30 - 7.26 (m, 1 H), 7.20 (d, *J* = 7.3 Hz, 1 H), 5.26 (q, *J* = 7.0 Hz, 1 H), 4.89 – 4.79 (m, 1 H), 1.66 (d, *J* = 6.8 Hz, 3 H), 1.51 (d, *J* = 6.8 Hz, 3 H), 1.46 (d, *J* = 6.8 Hz, 3 H); ^{13}C NMR (101 MHz, $CDCl_3$) δ 160.3, 154.0, 152.1, 143.7, 133.9, 128.6, 127.3, 126.1, 99.9, 50.6, 49.0, 22.60, 21.6, 21.5; IR (KBr, cm^{-1}): 3327, 2977, 1681, 1615, 1553, 1507, 1442, 1259, 1120, 782, 670; Anal. Calcd for $C_{16}H_{19}N_5O{\cdot}0.5H_2O$: C, 62.73; H, 6.58; N, 22.86; Found: C, 62.90; H, 6.34; N, 22.85.

*6-(benzyl(methyl)amino)-1-isopropyl-1,5-dihydro-4H-pyrazolo[3,4-d]pyrimidin-4-one (**H35**).* white solids (72 mg, yield: 80%). M.p.: 187-188 ºC; MS (ESI$^-$): *m/z*: 296 ([M-H]$^-$); ^{1}H NMR (500 MHz, DMSO-d_6) δ 10.66 (brs, 1H), 7.75 (s, 1H), 7.36 – 7.32 (m, 2H), 7.30 – 7.25 (m, 3H), 4.82 (s, 2H), 4.74 (hept, *J* = 6.7 Hz, 1H), 3.08 (s, 3H), 1.37 (d, *J* = 6.7 Hz, 6H); ^{13}C NMR (126 MHz, DMSO-d_6) δ 158.5, 153.3, 152.9, 137.3, 133.5, 128.4, 127.3, 127.1, 99.0, 52.4, 47.8, 35.7, 21.5; IR (KBr, cm^{-1}): 3120, 3050, 2979, 2934, 1676, 1595, 1544, 1387, 1285, 1113, 1003, 974, 815, 779, 729, 698; Anal. Calcd for $C_{16}H_{19}N_5O$: C, 64.63; H, 6.44; N, 23.55; Found: C, 64.59; H, 6.26; N, 23.43.

*(±)-6-((1-(4-chlorophenyl)ethyl)amino)-1-isopropyl-1,5-dihydro-4H-pyrazolo[3,4-d]pyrimidin-4-one (**H33**).* white solids (69 mg, yield: 69%). M.p.: 67-68 ºC; MS (ESI$^-$): *m/z*: 330 ([M-H]$^-$); ^{1}H NMR (400 MHz, $CDCl_3$) δ 10.70 (brs, 1H), 7.65 (s, 1H), 7.34 (d, *J* = 8.5 Hz, 2H), 7.30 – 7.26

Molecular Pharmacology Fast Forward. Published on August 27, 2015 as DOI: 10.1124/mol.115.099747
This article has not been copyedited and formatted. The final version may differ from this version.

(m, 2H), 7.14 (d, *J* = 7.0 Hz, 1H), 5.18 (q, *J* = 6.9 Hz, 1H), 4.73 – 4.79 (m, 1H), 1.61 (d, *J* = 7.0 Hz, 3H), 1.48 (d, *J* = 6.7 Hz, 3H), 1.41 (d, *J* = 6.7 Hz, 3H); ^{13}C NMR (101 MHz, $CDCl_3$) δ 160.3, 153.9, 152.0, 142.5, 133.7, 132.9, 128.7, 127.5, 99.9, 50.1, 49.0, 22.7, 21.6, 21.5; IR (KBr, cm^{-1}): 3321, 2977, 1681, 1615, 1553, 1444, 1259, 1092, 1013, 827, 781, 680; Anal. Calcd for $C_{16}H_{18}ClN_5O$: C, 57.92; H, 5.47; N, 21.11; Found: C, 58.20; H, 5.64; N, 20.76.

(±)-1-cyclopentyl-6-((1-phenylethyl)amino)-1,5-dihydro-4H-pyrazolo[3,4-d]pyrimidin-4-one ***(C10)***. white solids (78 mg, yield: 80%). M.p.: 172-174 ºC; MS (ESI^-): *m/z*: 322 ($[M-H]^-$); ^{1}H NMR (400 MHz, $CDCl_3$) δ 10.70 (brs, 1H), 7.58 (s, 1H), 7.45 – 7.39 (m, 2H), 7.36 – 7.31 (m 2H), 7.29 – 7.24 (m, 1H), 7.13 (d, *J* = 7.0 Hz, 1H), 5.25 (q, *J* = 6.8 Hz, 1H), 4.96 (p, *J* = 7.6 Hz, 1H), 2.12 – 2.05 (m, 2H), 2.05 – 1.98 (m, 2H), 1.97 – 1.88 (m, 2H), 1.75 – 1.67 (m, 2H), 1.65 (d, *J* = 6.9 Hz, 3H); ^{13}C NMR (101 MHz, $CDCl_3$) δ 160.3, 154.4, 152.1, 143.7, 133.9, 128.6, 127.3, 126.1, 99.9, 57.9, 50.6, 31.9, 31.7, 24.7, 24.7, 22.6; IR (KBr, cm^{-1}): 3317, 2960, 2868, 1680, 1615, 1555, 1443, 1258, 1121, 1066, 1012, 782, 698, 550; Anal. Calcd for $C_{18}H_{21}N_5O{\cdot}0.1\ H_2O$: C, 66.48; H, 6.57; N, 21.54; Found: C, 66.47; H, 6.44; N, 21.20.

6-(benzyl(methyl)amino)-1-cyclopentyl-1,5-dihydro-4H-pyrazolo[3,4-d]pyrimidin-4-one ***(C35)***. white solids (45 mg, yield: 46%). M.p.: 169-170 ºC; MS (ESI^-): *m/z*: 322 ($[M-H]^-$); ^{1}H NMR (400 MHz, DMSO-d_6) δ 7.76 (s, 1H), 7.39 – 7.23 (m, 5H), 4.96 – 4.86 (m, 1H), 4.82 (s, 2H), 3.08 (s, 3H), 2.03 – 1.76 (m, 6H), 1.67 – 1.56 (m, 2H); ^{13}C NMR (101 MHz, DMSO-d_6) δ 158.6, 153.4, 137.4, 133.7, 128.5, 127.4, 127.2, 99.1, 56.8, 52.4, 35.8, 31.6, 24.3; IR (KBr, cm^{-1}): 3112, 2953, 1865, 1593, 1566, 1546, 1388, 1358, 1293, 1055, 1004, 776, 705; Anal. Calcd for $C_{18}H_{21}N_5O{\cdot}0.4\ H_2O$: C, 65.39; H, 6.65; N, 21.18; Found: C, 65.79; H, 6.41; N, 20.84.

Molecular Pharmacology Fast Forward. Published on August 27, 2015 as DOI: 10.1124/mol.115.099747
This article has not been copyedited and formatted. The final version may differ from this version.

*(±)-6-((1-(4-chlorophenyl)ethyl)amino)-1-cyclopentyl-1,5,6,7-tetrahydro-4H-pyrazolo[3,4-d]pyrimidin-4-one (**C33**)*. white solids (49 mg, yield: 46%). M.p.: 209-210 ºC; MS (ESI$^-$): *m/z*: 356 ([M-H]$^-$); ^{1}H NMR (400 MHz, $CDCl_3$) δ 10.72 (brs, 1H), 7.64 (s, 1H), 7.36 – 7.32 (m, 2H), 7.30 – 7.26 (m, 2H), 7.07 (d, *J* = 7.1 Hz, 1H), 5.18 (q, *J* = 6.9 Hz, 1H), 4.90 (p, *J* = 7.5 Hz, 1H), 2.09 – 2.03 (m, 2H), 2.01 – 1.95 (m, 2H), 1.94 – 1.85 (m, 2H), 1.73 – 1.65 (m, 2H), 1.61 (d, *J* = 7.0 Hz, 3H); ^{13}C NMR (100 MHz, $CDCl_3$) δ 160.3 154.3, 151.9, 142.5, 133.7, 132.9, 128.7, 127.4, 99.9, 57.9, 50.1, 31.9, 31.7, 24.7, 22.9. IR (KBr, cm^{-1}): 3309, 2959, 2869, 1680, 1614, 1552, 1492, 1446, 1259, 1092, 1014, 825, 780. Anal. Calcd for $C_{18}H_{20}ClN_5O$: C, 60.42; H, 5.63; N, 19.57; Found: C, 60.44; H, 5.84; N, 19.28.

*(R)-6-((1-(4-chlorophenyl)ethyl)amino)-1-cyclopentyl-1,5,6,7-tetrahydro-4H-pyrazolo[3,4-d]pyrimidin-4-one ((R)-**C33**)*. white solids (56 mg, yield: 52%).MS (ESI$^-$): *m/z*: 356 ([M-H]$^-$); ^{1}H NMR (400 MHz, $CDCl_3$) δ 10.74 (brs, 1H), 7.66 (s, 1H), 7.38 – 7.34 (m, 2H), 7.33 – 7.27 (m, 2H), 7.18 (d, *J* = 6.9 Hz, 1H), 5.21 (q, *J* = 6.9 Hz, 1H), 4.94 (p, *J* = 7.5 Hz, 1H), 2.12 – 1.91 (m, 6H), 1.77 – 1.68 (m, 2H), 1.64 (d, *J* = 7.0 Hz, 3H). ^{13}C NMR (100 MHz, $CDCl_3$) δ 160.3, 154.3, 151.9, 142.4, 133.7, 132.9, 128.7, 127.4, 99.9, 57.9, 50.1, 32.0, 31.7, 24.8, 24.7, 22.8. Anal. Calcd for $C_{18}H_{20}ClN_5O$: C, 60.42; H, 5.63; N, 19.57; Found: C, 60.18; H, 5.68; N, 19.39. $[\alpha]_D^{20}$ = +92 (c = 1 g/L, $CHCl_3$).

(S)-6-((1-(4-chlorophenyl)ethyl)amino)-1-cyclopentyl-1,5,6,7-tetrahydro-4H-pyrazolo[3,4-d]pyrimidin-4-one ((S)-C33). white solids (52 mg, yield: 49%). MS (ESI$^-$): *m/z*: 356 ([M-H]$^-$); ^{1}H NMR (400 MHz, $CDCl_3$) δ 10.71 (s, 1H), 7.66 (s, 1H), 7.40 – 7.34 (m, 2H), 7.34 – 7.29 (m, 2H),

Molecular Pharmacology Fast Forward. Published on August 27, 2015 as DOI: 10.1124/mol.115.099747
This article has not been copyedited and formatted. The final version may differ from this version.

7.24 (d, *J* = 7.0 Hz, 1H), 5.21 (q, *J* = 6.9 Hz, 1H), 4.94 (p, *J* = 7.5 Hz, 1H), 2.13 – 1.90 (m, 6H), 1.75 – 1.67 (m, 2H), 1.64 (d, *J* = 7.0 Hz, 3H). ^{13}C NMR (100 MHz, $CDCl_3$) δ 160.3, 154.3, 151.9, 142.5, 133.7, 132.9, 128.7, 127.4, 99.9, 57.9, 50.0, 32.0, 31.7, 24.8, 24.7, 22.8. Anal. Calcd for $C_{18}H_{20}ClN_5O$: C, 60.42; H, 5.63; N, 19.57; Found: C, 60.54; H, 5.66; N, 19.71. $[\alpha]_D^{20}$ = -93 (c = 1 g/L, $CHCl_3$).

*(±)-6-((1-(4-chlorophenyl)-2-methylpropyl)amino)-1-cyclopentyl-1,5,6,7-tetrahydro-4H-pyrazolo[3,4-d]pyrimidin-4-one (**C40**).* white solids (79 mg, yield: 68%). M.p. 210-212 ºC. MS (ESI⁻): *m/z*: 386 ([M-H]⁻); ^{1}H NMR (400 MHz, DMSO-d_6) δ 10.23 (s, 1H), 7.72 (s, 1H), 7.37 (m, 4H), 7.08 (s, 1H), 4.88 – 4.77 (m, 1H), 4.70 – 4.65 (m, 1H), 2.07 – 2.03 (m, 1H), 2.01 – 1.73 (m, 6H), 1.70 – 1.49 (m, 2H), 0.95 (d, *J* = 6.7 Hz, 3H), 0.82 (d, *J* = 6.7 Hz, 3H). ^{13}C NMR (126 MHz, $CDCl_3$) δ 160.3, 154.4, 152.4, 140.6, 133.8, 132.7, 128.4, 128.3, 99.8, 60.8, 57.7, 33.8, 32.0, 31.6, 24.7, 24.7, 19.9, 19.2. IR (KBr, cm^{-1}): 3344, 2931, 2852, 1689, 1610, 1552, 1506, 1491, 1441, 1265, 1251, 1089, 1051, 1012, 989, 827, 816, 781, 621, 581, 557. Anal.Calcd for $C_{20}H_{24}ClN_5O{\cdot}0.15H_2O$: C, 61.82; H, 6.30; N, 18.02; Found: C, 62.11; H, 6.12; N, 17.74.

*(±)-1-isobutyl-6-((1-phenylethyl)amino)-1,5-dihydro-4H-pyrazolo[3,4-d]pyrimidin-4-one (**K10**).* white solids (52 mg, yield: 54%). M.p.: 84-85 ºC; MS (ESI⁻): *m/z*: 310 ([M-H]⁻); ^{1}H NMR (400 MHz, $CDCl_3$) δ 10.66 (brs, H), 7.48 (s, H), 7.43 – 7.39 (m, 2H), 7.36 – 7.29 (m, 2H), 7.29 – 7.21 (m, 1H), 7.16 (d, *J* = 6.9 Hz, 1H), 5.20 (q, *J* = 6.8 Hz, 1H), 4.00 – 3.88 (m, 2H), 2.28 – 2.11 (m, 1H), 1.64 (d, *J* = 6.9 Hz, 3H), 0.88 (d, *J* = 6.7 Hz, 3H), 0.81 (d, *J* = 6.7 Hz, 3H); ^{13}C NMR (101 MHz, $CDCl_3$) δ 160.3, 155.1, 152.3, 143.7, 134.1, 128.6, 127.3, 126.2, 99.4, 54.1, 50.7, 28.9, 22.4, 20.0, 19.9; IR (KBr, cm^{-1}): 3489, 3268, 2962, 1680, 1611, 1566, 1520, 1457, 1277, 1094,

Molecular Pharmacology Fast Forward. Published on August 27, 2015 as DOI: 10.1124/mol.115.099747
This article has not been copyedited and formatted. The final version may differ from this version.

882, 756, 699, 554, 476; Anal. Calcd for $C_{17}H_{21}N_5O \cdot 0.3H_2O$: C, 64.45; H, 6.87; N, 22.11; Found: C, 64.71; H, 7.06; N, 21.86.

6-(benzyl(methyl)amino)-1-isobutyl-1,5-dihydro-4H-pyrazolo[3,4-d]pyrimidin-4-one (***K35***). white solids (39 mg, yield: 42%). M.p.: 187-188 ºC; MS (ESI$^-$): *m/z*: 310 ([M-H]$^-$); ^{1}H NMR (400 MHz, DMSO-d_6) δ 7.78 (s, 1H), 7.37 – 7.22 (m, 5H), 4.80 (s, 2H), 3.88 (d, *J* = 7.1 Hz, 2H), 3.08 (s, 3H), 2.16 – 2.05 (m, 1H), 0.79 (d, *J* = 6.7 Hz, 6H); ^{13}C NMR (101 MHz, DMSO-d_6) δ 159.2, 154.6, 153.9, 138.0, 134.4, 128.9, 127.9, 127.7, 99.0, 53.5, 53.0, 36.3, 29.0, 20.2; IR (KBr, cm^{-1}): 3117, 2958, 1692, 1580, 1453, 1387, 1314, 1157, 1056, 1013, 884, 809, 780, 699, 627, 563, 474; Anal. Calcd for $C_{17}H_{21}N_5O$: C, 65.57; H, 6.80; N, 22.49; Found: C, 65.56; H, 6.76; N, 22.30.

(±)-6-((1-(4-chlorophenyl)ethyl)amino)-1-isobutyl-1,5-dihydro-4H-pyrazolo[3,4-d]pyrimidin-4-one (**K33**). white solids (61 mg, yield: 58%). M.p.: 88-89 ºC; MS (ESI$^-$): *m/z*: 344 ([M-H]$^-$); ^{1}H NMR (400 MHz, $CDCl_3$) δ 10.79 (brs, 1H), 7.65 (s, 1H), 7.34 – 7.27 (m, 4H), 6.88 (d, *J* = 6.7 Hz, 1H), 5.13 (q, *J* = 6.8 Hz, 1H), 3.96 – 3.85 (m, 2H), 2.21 – 2.10 (m, 1H), 1.61 (d, *J* = 7.0 Hz, 3H), 0.87 (d, *J* = 6.7 Hz, 3H), 0.79 (d, *J* = 6.7 Hz, 3H); ^{13}C NMR (101 MHz, $CDCl_3$) δ 160.4, 155.0, 152.0, 142.5, 134.0, 132.9, 128.7, 127.4, 99.5, 54.2, 50.3, 28.9, 22.7, 20.0, 19.8; IR (KBr, cm^{-1}): 3429, 3270, 2964, 2930, 1678, 1608, 1560, 1516, 1458, 1401, 1318, 1270, 1171, 1094, 1014, 824, 780, 589, 539; Anal. Calcd for $C_{17}H_{20}ClN_5O \cdot 0.9H_2O$: C, 56.40; H, 6.07; N, 19.34; Found: C, 56.48; H, 6.14; N, 19.12.

Protein expression and purification

Molecular Pharmacology Fast Forward. Published on August 27, 2015 as DOI: 10.1124/mol.115.099747
This article has not been copyedited and formatted. The final version may differ from this version.

The PDE9A2 catalytic domain (residues 181-506) was subcloned to vector pET15b and purified according to the protocols described by Huai et al. (2004). Briefly, the pET15-PDE9 plasmid was transferred into *E. coli.* strain BL21 (Codonplus, Stratagene) for overexpression. When the *E. coli.* cell was grown in LB medium at 37 ºC to absorption A600 = 0.7, 0.1 mM isopropyl β-D-thiogalactopyranoside was added to induce the expression at 15 ºC overnight. Recombinant PDE9A2 protein was purified by column chromatography of Ni-NTA (GE Healthcare), Q-sepharose (GE), and Superdex-200 (GE). A typical batch of purification yielded 20–60 mg PDE9A2 from a liter cell culture. The PDE9A2 protein has purity >90% as judged by SDS-PAGE.

The catalytic domains of PDE2A3 (222-904), PDE4D2 (86-413), PDE5A1 (535-860), PDE7A1 (130-482), PDE8A2 (480-820), and PDE10A2 (448-789) were purified by published protocols (Huai et al., 2003; Wang et al 2005; 2006; 2007a; 2008a). PDE1B (10-516) was expressed and purified using a protocol similar to that for PDE9.

Enzymatic assay

The enzymatic activities of PDE9A2 and other PDEs were assayed by using ^{3}H-cGMP or ^{3}H-cAMP as the substrate. The assay buffer was composed of 50 mM Tris-HCl pH 8.0, 10 mM $MgCl_2$ or 4 mM $MnCl_2$, 1 mM DTT, and 20 nM ^{3}H-cGMP or ^{3}H-cAMP (20,000–30,000 cpm/assay, GE Healthcare). The reaction was carried out at room temperature for 15 min and then terminated by addition of 0.2 M $ZnSO_4$. The reaction products ^{3}H-GMP or ^{3}H-AMP were precipitated by adding 0.2 N $Ba(OH)_2$, whereas the unreacted ^{3}H-cGMP or ^{3}H-cAMP remained in the supernatant. Radioactivity in the supernatant was measured in 2.5 mL Ultima Gold liquid scintillation cocktails by a liquid scintillation counter. The final concentrations of the enzymes

Molecular Pharmacology Fast Forward. Published on August 27, 2015 as DOI: 10.1124/mol.115.099747
This article has not been copyedited and formatted. The final version may differ from this version.

used in the assay were 50-200 ng/mL and hydrolyzed up to 70% of the substrates. Nine to twelve concentrations of inhibitors were used for a triplet measurement of IC_{50} and the standard deviations that were obtained by nonlinear regression.

Crystallization and structure determination

The crystals of the PDE9A2 catalytic domain (181−506) in complex with racemic **C33** and the (R)- and (S)-enantiomers were grown by the hanging drop vapor diffusion method. The PDE9A2 (8-10 mg/mL) in a buffer of 50 mM NaCl, 20 mM Tris·HCl, pH 7.5, 1 mM β-mercaptoethanol, and 1 mM EDTA was mixed with 2 mM racemic **C33** or (R)-**C33** and co-crystallized against a well buffer of 1.8 - 2.0 M sodium formate at 4 ºC. The PDE9-(S)-**C33** crystals were prepared by soaking of the PDE9-IBMX crystals in the crystallization buffer plus 2 mM (S)-**C33** at 25 ºC for 1 day. The PDE9-IBMX crystals were grown by hanging drop against a well buffer of 0.1 M HEPES pH 7.5, 3.0 M sodium formate at 4 ºC. The crystallization buffer plus 20% glycerol was used as the cryosolvent to freeze crystals. X-ray diffraction data were collected on beamline X29 in Brookhaven National Laboratory (for racemic **C33**) or BM22 of SER-CAT of Advanced Photon Source at Chicago (for (R)-**C33** and (S)-**C33)**, and processed by HKL 2000 (Otwinowski et al., 1997). The structures were solved by molecular replacement, using the PDE9A2 catalytic domain as the initial model. The resulting models were rebuilt by program COOT (Emsley et al., 2010) and refined by REFMAC (Winn et al., 2003). The statistics of data collection and structure refinement are listed in Table 1.

Pharmacokinetics analysis

Molecular Pharmacology Fast Forward. Published on August 27, 2015 as DOI: 10.1124/mol.115.099747
This article has not been copyedited and formatted. The final version may differ from this version.

Six male Sprague Dawey rats with body weight of 240-275 g were used for the pharmacokinetic experiments. Compound **C33** was dissolved in 5% DMSO, 5% solutol, and 90% saline to make a 5 mg/mL stock for intravenous administration (IV) and 1 mg/mL for oral administration (PO). A final dosage of 5 mg/kg formulated compound was given in both administration modes. The blood samples were taken at various time points in 24 hours. The concentration of the compounds in blood was analyzed by LC-MS/MS (Shimadzu liquid chromatographic system, and API4000 mass spectrometer, Applied Biosystems, Ontario, Canada).

Stability in liver microsomes

Warfarin and testosterone was purchased from Sigma (St. Louis, MO, USA) and Acros (Geel, Belgium), respectively. Human and mouse (CD-1) liver microsomes (0.5 mL, BD Gentest Corporation, Woburn, MA, USA) were pre-incubated with 0.75 µM sample in a buffer of 0.1 M potassium phosphate pH 7.4, and 2 mM $MgCl_2$ in a 96-well plate at 37 ºC for 5 min. The enzymatic reaction was initiated by adding 3 mM NADPH and terminated by adding 90 µL acetonitrile at time points of 0, 5, 10, 20, and 30 min. Parallel incubations were performed for the positive (testosterone) and negative (warfarin) controls. The supernatant was injected into LC-MS/MS for analysis.

RESULTS

Structure-based design and enzymatic activity of PDE9 inhibitors

We previously reported a potent PDE9 inhibitor **3r** (Fig. 1), which has an IC_{50} of 0.6 nM against PDE9, but only a moderate metabolic stability and 10% bioavailability (Shao et al.,

Molecular Pharmacology Fast Forward. Published on August 27, 2015 as DOI: 10.1124/mol.115.099747
This article has not been copyedited and formatted. The final version may differ from this version.

2014). To improve the *in vivo* stability, we designed a series of analogues of **3r** and docked them to the PDE9 crystal structures for confirmation. Since **3r** contains an amide bond that is often labile to acids and proteinases and may thus account for its moderate bioavailability, we removed the amide unit of **3r** and also optimized the tail group with hydrocarbon fragments. Removal of the amide group would be expected to lead to a loss of the hydrogen bond between the amide nitrogen of the inhibitor and OH of Tyr424 and thus to sacrifice somewhat affinity and selectivity because Tyr424 is the unique residue for PDE8 and PDE9 (phenylalanine in other PDE families). However, if the pyrazolopyrimidinone and cyclic pentanyl groups that contribute the hydrogen bonds with the invariant glutamine and hydrophobic stack against the phenylalanine are retained as the scaffold of pharmacophore, optimization of the remaining moiety may lead to finding of new compounds with practically reasonable affinity and selectivity. In addition, since the benzenylamine link is usually sensitive to P450 metabolic enzymes *in vivo*, we hope that introduction of N-alpha substitutent would protect oxidation of benzenylamine to benzamide. Thus we rationally designed a series of new compounds on basis of the crystal structures of PDEs and performed molecular docking to confirm the design. Compounds from this rational design and docking are then chemically synthesized and assayed for their enzymatic properties. The inhibition of some representative compounds on PDE9 is listed in Table 2, among which racemic **C33** shows the best IC_{50} of 16 nM against PDE9. Overall, the IC_{50} values of the listed compounds are not dramatically different, perhaps due to that the modified groups target the similar protein regions and interact with similar residues.

Based on the observation that the methyl group on the chiral carbon is neighboring a small hydrophobic pocket in the PDE9-**r3** crystal structure (Shao et al., 2014), we hope that the tail of (R)- or (S)-**C33** may interact with the hydrophobic pocket so as to further improve the

Molecular Pharmacology Fast Forward. Published on August 27, 2015 as DOI: 10.1124/mol.115.099747
This article has not been copyedited and formatted. The final version may differ from this version.

affinity and selectivity. Therefore, racemic and enantiomeric **C33**s were chemically synthesized and their inhibitions on PDE families were evaluated (Table 3). The enzymatic assay revealed that racemic, (S)- and (R)-**C33** have the IC_{50} values of 16, 11, and 56 nM for inhibition on the PDE9 catalytic domain, respectively, and (S)-**C33** has a reasonably good selectivity over other PDE families (Table 3), indicating its potential for further pharmacological studies.

Improvement in bioavailability and stability in live microsomes

While IC_{50} of 11nM of (S)-**C33** is in the IC_{50} range of most drugs, it is significantly worse than 0.6 nM of **3r** and also the enzymatic selectivity of (S)-**C33** over other PDE families significantly decreases. However, in terms of bioavailability and *in vivo* stability, **C33** shows significant improvement over **3r**. The oral administration of racemic **C33** yielded Cmax of 373 ng/mL and bioavailability of 56.5% (Table 4), in comparison with Cmax of 16 ng/mL and 217 ng/mL and bioavailability of 1.3% and 9.8% respectively for **28s** (Meng et al., 2012) and **3r** (Shao et al., 2014). The blood concentration of **C33** in the oral administration mode was 113 ng/mL at the 6^{th} hour, which is about 19 fold higher than the IC_{50} of 6 ng/mL, indicating practical usability and the potential of **C33** as a drug lead. In addition, the replacement of the amide bond with a hydrocarbon fragment in **C33** yields stronger hydrophobicity than **3r**, as shown by a LogP of 3.59 **C33** in comparison to LogP of 1.86 for **3r**, implying a strong ability to penetrat cell membrane.

In addition, the metabolic stability of **C33** in human and mouse liver microsomes suggests that **C33** may have better *in vivo* stability than **3r**. Apparently, the removal of the amide group from **3r** significantly improved the stability, as shown by the T½ values of 51 and 12 minutes respectively for racemic **C33** and **3r** in the human liver microsome, and of 33 and 22

Molecular Pharmacology Fast Forward. Published on August 27, 2015 as DOI: 10.1124/mol.115.099747
This article has not been copyedited and formatted. The final version may differ from this version.

minutes in the mouse liver microsome (Table 5). In the enantiomeric forms of **C33**, (S)-**C33** is apparently more stable than (R)-**C33**, as shown by T½ values of 105 and 54 minutes in human and mouse microsomes for **(S)-C33**, in comparison with 44 and 22 minutes for (R)-**C33**. The explanation is not clear, but may be related to their different conformations and interactions.

On the other hand, we replaced the methyl group of **C33** with an isopropanyl group to seek a spatial obstacle for protection of the C-N bond, and thus lead to design of **C40** (Fig. 1). Indeed, the stability of **C40** was significantly improved, as shown by $T_{1/2}$ of 62 and 291 minutes respectively in the human and mouse liver microsomes (Table 5), although IC_{50} of **C40** against PDE9 was increased to 73.5 nM.

Asymmetry of PDE9 dimers

The crystallographic asymmetric units of PDE9 in complex with racemic or enantiomeric **C33** contain two molecules of the PDE9 catalytic domain (Fig. 2). Superposition of subunit A over B in the PDE9-**C33** dimer yielded a root mean square deviation (RMSD) of 0.62 Å for Cα atoms of the whole domain (residues 185-506). A systematic superposition of subunit A over B of other PDE9 structures in the RCSB Protein Data Bank resulted in RMSDs in a range of 0.55 and 0.78 Å for Cα atoms of residues 185 - 506. These small RMSDs indicate overall similarity between two subunits of the PDE9 dimers. On the other hand, superposition of PDE9-**C33** over other PDE9 structures yielded RMSDs of 0.27 – 0.49 and 0.22 – 0.42 Å respectively for comparison of A versus A and B versus B. Similar RMSDs were obtained from the cross superposition among other PDE9 structures. Since a superposition between structures reported from different laboratories often produces higher RMSDs than a comparison between subunits

Molecular Pharmacology Fast Forward. Published on August 27, 2015 as DOI: 10.1124/mol.115.099747
This article has not been copyedited and formatted. The final version may differ from this version.

within the same structure, the consistently and significantly larger RMSDs for A ~ B in the same dimers than A ~ A or B ~ B between different structures suggest asymmetry of the PDE9 dimers.

When the N- and C-terminal residues were excluded, the superposition between residues 192-486 of the PDE9-**C33** dimer yielded RMSD of 0.17 Å for the Cα atoms, suggesting flexibility of the N- and C-termini. A careful examination of the superposition revealed RMSDs of 0.25 – 0.62 Å for residues 432-440 (the M-loop), which are 1.5 - 4 fold to the overall average of 0.17 Å for residues 192-486, suggesting significant conformational differences between two M-loops in the PDE9 dimer. A systematic comparison between subunits A and B of the PDE9 structures in the Protein Data Bank reveals the average difference between the Cα atoms of the M-loop in the dimer is about twice the overall average of the PDE9 catalytic domain (Table 6), thus confirming the asymmetry the M-loop. While the N- and C-termini have the largest RMSD differences, their biological relevance is unclear because terminal flexibility is often due to lack of lattice packing in many crystal structures. However, the difference between the M-loops of PDE9 dimers is statistically significant and appears to be biologically relevant.

The asymmetry of PDE9 dimer was first observed in the crystal structure of the PDE9 catalytic domain in complex with inhibitor 3-isobutyl-1-methylxanthine (IBMX), in which two IBMX molecules bind the active sites of the PDE9 dimer with different orientations (Huai et al., 2004). Later, it was shown that substrate cGMP or product GMP easily replaced IBMX in subunit A of the PDE9-IBMX dimer in the soaking experiments, but not the IBMX in subunit B (Liu et al., 2008). Finally, the asymmetry was reported for the binding of inhibitor BAY73-6691 to the Q453E mutant (Hou et al., 2011). The subtle conformational asymmetry of the M-loop, which is revealed by this study, may respond to the asymmetric binding/replacement of the inhibitors.

Molecular Pharmacology Fast Forward. Published on August 27, 2015 as DOI: 10.1124/mol.115.099747
This article has not been copyedited and formatted. The final version may differ from this version.

Different conformations of bound C33 enantiomers

In the structure of PDE9 in complex with racemic **C33**, the electron density in the maps of (2Fo - Fc) and (Fo - Fc) revealed binding of (S)-**C33** enantiomer to subunits A and (R)-**C33** to subunit B of the PDE9 dimer (Fig. 3). In the structures of PDE9 in complex with enantiomerically pure (S)-**C33** or (R)-**C33**, the maps showed unique conformations of (S)-**C33** and (R)-**C33** bound to both subunits A and B of their PDE9 dimers. These conformations are identical respectively to that of (S)- or (R)-enantiomer in the racemic **C33**-PDE9 complex.

The pyrazolopyrimidinone and cyclic pentanyl rings of **C33** in all three structures had the same conformation and were well superimposable. The pyrazolopyrimidinone rings of **C33** formed two hydrogen bonds with invariant Gln453 and aromatic π-stack against Phe456, in addition to the hydrophobic interactions with Leu420 and Ala452. The nitrogen linked to pyrazolopyrimidinone formed a hydrogen bond with the carbonyl oxygen of Ala452. The cyclic pentanyl rings of racemic or enantiomeric **C33** occupied the same location near the metal binding pocket and contacted Met365 and Tyr424. However, the chlorophenyl tails of (S)-**C33** and (R)-**C33** oriented to different directions so as to define the different bound conformations of two enantiomers in the PDE9 dimers (Fig. 3). The chlorophenyl tail of (S)-**C33** interacted with a small hydrophobic pocket, which we tentatively name as the M-pocket (see discussion later), and contacted residues of Leu420, Leu421, Tyr424, Phe441, Met442, Ala452, and Phe456. In comparison, the chlorophenyl tail of (R)-**C33** pointed out the molecular surface and contacted residues of Leu420, Tyr424, Phe441, Ala452, and Phe456 (Fig. 3C). Apparently, the (S)-**C33** tail makes more van der Waals interactions with PDE9 than (R)-**C33**, thus explaining its slightly better binding affinity.

Molecular Pharmacology Fast Forward. Published on August 27, 2015 as DOI: 10.1124/mol.115.099747
This article has not been copyedited and formatted. The final version may differ from this version.

Since the link between the chiral carbon and the nitrogen (Fig. 1) is a single bond, free rotation of the bond might produce an orientation of the (R)-**C33** tail in a similar conformation as (S)-**C33** to interact with the M-pocket. However, the crystal structure revealed that the chlorobenzyl tail of (R)-**C33** oriented to the molecular surface of the PDE9 dimer, instead of interacting with the M-pocket. The different conformations and interactions of the tails of (S)- and (R)-**C33** enantiomers might be impacted by the subtle asymmetry of the M-pocket in the PDE9 dimer. Therefore, the structural information suggests that both subunits of the PDE9 dimer need to be considered for design of PDE9 inhibitors.

DISCUSSION

An important subpocket for selectivity of PDE inhibitors

The early studies on the crystal structures of PDE9 in complex with BAY73-6691 (Wang et al., 2010) and **28s** (Meng et al., 2012) showed a small pocket neighboring the inhibitor binding site. This study revealed that the chlorophenyl tail of inhibitor (S)-**C33** interacts with the small subpocket that is composed of a portion of helices H14 and H15 and the M-loop and thus we tentatively name as the M-pocket (Fig. 4). Helices H14 (Leu420, Leu421 and Phe425) and H15 contribute two walls of the pocket, while Val447 and backbone of the M-loop form the bottom of the pocket. This small pocket is gated by Ala452 of H15 and Phe441 of the M-loop and occupies the similar location as the P-pocket in the parasite PDEs. Sequence alignment reveals that the gating residues vary significantly across PDE families (Fig. 4C) so as to make the pocket inaccessible in many human PDEs (Wang et al., 2007b; 2012).

In addition, the M-loop shows significant differences in sequence and conformations (Fig. 4) and is disordered in some PDE families. Therefore, we believe that the M-pocket may

Molecular Pharmacology Fast Forward. Published on August 27, 2015 as DOI: 10.1124/mol.115.099747
This article has not been copyedited and formatted. The final version may differ from this version.

serve as a selectivity determinant for inhibitors binding and is useful for improvement of inhibitor affinity and selectivity. For example, the M-pocket in PDE5, which is composed of Val782, Ala783, Phe786, Phe787 and Ile813 (Fig. 5A), is slightly deeper than that of PDE9. However, two large gating residues of Leu804 and Met816 would allow small group to penetrate into the pocket, such as an ethoxyl fragment in the PDE5-sildenafil structure (Wang et al., 2008b). This might explain why (S)-**C33** has better selectivity than (R)-**C33** against PDE5 (Table 2). The M-pocket in the PDE8A1 structure, which is made up of residues Ser745, Tyr748, Phe749, Phe767, and Cys772, is much shallower and smaller than that of PDE9 and might not well accommodate the **C33** inhibitors (Fig. 5B), thus explaining poor binding of **C33** to PDE8. In the structure of PDE1, the M-loop has a good conservation of amino acids, as shown by correspondence of Leu388, Met389, and Phe392 of PDE1B to Leu420, Leu421, and Y424 of PDE9, respectively. Since part of the M-pocket is disordered in PDE1, it might reasonably predict a poor selectivity of PDE9 inhibitors against PDE1, as observed in the PDE9 structure (Wunder et al., 2005).

Acknowledgment

Diffraction data were collected at beamline X29A at Brookhaven National Laboratory and Southeast Regional Collaborative Access Team (SER-CAT) 22-BM beamline at the Advanced Photon Source, Argonne National Laboratory.Supporting institutions may be found at www.ser-cat.org/members.html. Use of the Advanced Photon Source was supported by the U. S. Department of Energy, Office of Science, Office of Basic Energy Sciences, under Contract No. W-31-109-Eng-38.

Molecular Pharmacology Fast Forward. Published on August 27, 2015 as DOI: 10.1124/mol.115.099747
This article has not been copyedited and formatted. The final version may differ from this version.

Authorship contributions

Participated in research design: Y. Wan, P. Liu, H. Ke, H. Luo.

Conducted experiments: M. Huang, J. Hou, Y. Shao, Y. Wu., Cui, B. Liang.

Performed data analysis: M. Huang, Y. Shao, W. Cui, B. Liang, Z. Li, X. Zhu, Y. Huang.

Wrote or contributed to the writing of the manuscript: Y. Wan, H. Ke, H. Luo.

References

Agranat I, Caner H, and Caldwell J (2002) Putting chirality to work: the strategy of chiral switches. *Nat Rev Drug Discov* **1**:753-768.

Claffey MM, Helal CJ, Verhoest PR, Kang Z, Bundesmann MW, Hou X, Lui S, Kleiman RJ, Vanase-Frawley M, Schmidt AW, Menniti F, Schmidt CJ, Hoffman WE, Hajos M, McDowell L, O'Connor RE, MacDougall-Murphy M, Fonseca KR, Becker SL, Nelson FR, and Liras S (2012) Application of structure-based drug design and parallel chemistry to identify selective, brain penetrant, in vivo active phosphodiesterase 9A inhibitors. *J Med Chem* **55**:9055-9068.

Conti M and Beavo J (2007) Biochemistry and physiology of cyclic nucleotide phosphodiesterases: essential components in cyclic nucleotide signaling. *Annu Rev Biochem* **76**:481-511.

Deninno MP, Andrews M, Bell AS, Chen Y, Eller-Zarbo C, Eshelby N, Etienne JB, Moore DE, Palmer MJ, Visser MS, Yu LJ, Zavadoski WJ, and Michael Gibbs E (2009) The discovery of potent, selective, and orally bioavailable PDE9 inhibitors as potential hypoglycemic agents. *Bioorg Med Chem Lett* **19**:2537-2541.

Emsley P, Lohkamp B, Scott WG, and Cowtan K (2010) Features and development of Coot. *Acta Cryst* **66**:486-501.

Heckman PRA, Wouters C, and Prickaerts J (2015) Phosphodiesterase inhibitors as a target for cognition enhancement in aging and alzheimerμs disease: A translational overview. *Curr Pharm Des* **21**:317-331.

Hou J, Xu J, Liu M, Zhao R, Luo H-B, and Ke H (2011) Structural asymmetry of phosphodiesterase-9, potential protonation of a glutamic acid, and role of the invariant glutamine. *PLoS One* **6**:e18092.

Huai Q, Wang H, Sun Y, Kim H-Y, Liu Y, and Ke H (2003) Three-dimensional structures of PDE4D in complex with roliprams and implication on inhibitor selectivity. *Structure* **11**:865-873.

Huai Q, Wang H, Zhang W, Colman RW, Robinson H, and Ke H (2004) Crystal structure of phosphodiesterase 9 shows orientation variation of inhibitor 3-isobutyl-1-methylxanthine binding. *Proc Natl Acad Sci U S A* **101**:9624-9629.

Hutson PH, Finger EN, Magliaro BC, Smith SM, Converso A, Sanderson PE, Mullins D, Hyde LA, Eschle BK, Turnbull Z, Sloan H, Guzzi M, Zhang X, Wang A, Rindgen D, Mazzola R, Vivian JA, Eddins D, Uslaner JM, Bednar R, Gambone C, Le-Mair W, Marino MJ, Sachs N, Xu G, and Parmentier-Batteur S (2011) The selective phosphodiesterase 9 (PDE9) inhibitor PF-04447943 (6-[(3S,4S)-4-methyl-1-(pyrimidin-2-ylmethyl)pyrrolidin-3-yl]-1-(tetrahydro-2H-pyran-4-yl)-1,5-dihydro-4H-pyrazolo[3,4-d]pyrimidin-4-one) enhances synaptic plasticity and cognitive function in rodents. *Neuropharmacology* **61**:665-676.

Kleiman RJ, Chapin DS, Christoffersen C, Freeman J, Fonseca KR, Geoghegan KF, Grimwood S, Guanowsky V, Hajos M, Harms JF, Helal CJ, Hoffmann WE, Kocan GP, Majchrzak MJ, McGinnis D, McLean S, Menniti FS, Nelson F, Roof R, Schmidt AW, Seymour PA, Stephenson DT, Tingley FD, Vanase-Frawley M, Verhoest PR, and Schmidt, CJ (2012) Phosphodiesterase 9A regulates central cGMP and modulates responses to cholinergic and monoaminergic perturbation in vivo. *J Pharmacol Exp Ther* **341**:396-409.

Kroker KS, Rast G, Giovannini R, Marti A Dorner-Ciossek C, and Rosenbrock H (2012) Inhibition of acetylcholinesterase and phosphodiesterase-9A has differential effects on hippocampal early and late LTP. *Neuropharmacology* **62**:1964-1974.

Kroker KS, Mathis C, Marti A, Cassel J-C, Rosenbrock H, Dorner-Ciossek C (2014) PDE9A inhibition rescues amyloid beta-induced deficits in synaptic plasticity and cognition. *Neurobiol Aging* **35**:2072-2078.

Liddie S, Anderson KL, Paz A, and Itzhak Y (2012) The effect of phosphodiesterase inhibitors on the extinction of cocaine-induced conditioned place preference in mice. *J Psychopharmacol* **26**:1375-1382.

Liu S, Mansour MN, Dillman KS, Perez JR, Danley DE, Aeed PA, Simons SP, Lemotte PK, and Menniti FS (2008) Structural basis for the catalytic mechanism of human phosphodiesterase 9. *Proc Natl Acad Sci U S A* **105**:13309-13314.

Londesborough J (1985) Evidence that the peripheral cyclic AMP phosphodiesterase of rat liver plasma membranes is a metalloenzyme. *Biochem J* **225**:143-147.

Maurice DH, Ke H, Ahmad F, Wang Y, Chung J, Manganiello VC (2014) Advances in targeting cyclic nucleotide phosphodiesterases. *Nat Rev Drug Discov* **13**:290-314.

Meng F, Hou J, Shao YX, Wu PY, Huang M, Zhu X, Cai Y, Li Z, Xu J, Liu P, Luo HB, Wan Y, and Ke H (2012) Structure-based discovery of highly selective phosphodiesterase-9A inhibitors and implications for inhibitor design. *J Med Chem* **55**:8549-8558.

Mentel M, Blankenfeldt W, and Breinbauer R (2009) The active site of an enzyme can host both enantiomers of a racemic ligand simultaneously. *Angew Chem Int Ed* **48**:9084-9087.

Nagy D, Tingley FD, 3rd, Stoiljkovic M, and Hajos M (2015) Application of neurophysiological biomarkers for Huntington's disease: evaluating a phosphodiesterase 9A inhibitor. *Exp Neurol* **263**:122-131.

Otwinowski Z and Minor W. (1997) Processing of x-ray diffraction data collected in oscillation mode. *Methods Enzymol* **276**:307-326.

Schwam EM, Nicholas T, Chew R, Billing CB, Davidson W, Ambrose D, and Altstiel LD (2014) A multicenter, double-blind, placebo-controlled trial of the PDE9A inhibitor, PF-04447943, in Alzheimer's disease. *Curr Alzheimer Res* **11**:413-421.

Sekhon BS (2013) Exploiting the power of stereochemistry in drugs: an overview of racemic and enantiopure drugs. *J Mod Med Chem* **1**:10-36.

Shaner NC, Steinbach PA, and Tsien RY (2005) A guide to choosing fluorescent proteins. *Nat Methods* **2**:905-909.

Shao Y-x, Huang M, Cui W, Feng L-J, Wu Y, Cai Y, Li Z, Zhu X, Liu P, Wan Y, Ke H, and Luo HB (2014) Discovery of a phosphodiesterase 9Ainhibitor as a potential hypoglycemic agent. *J Med Chem* **57**:10304-10313.

Singh N and Patra S (2014) Phosphodiesterase 9: insights from protein structure and role in therapeutics. *Life Sci* **106**:1-11.

van der Staay FJ, Rutten K, Baerfacker L, DeVry J, Erb C, Heckroth H, Karthaus D, Tersteegen A, van Kampen M, Blokland A, Prickaerts J, Reymann KG, Schroeder UH, and Hendrix M (2008) The novel selective PDE9 inhibitor BAY 73-6691 improves learning and memory in rodents. *Neuropharmacology* **55**:908-918.

Vardigan JD, Converso A, Hutson PH, and Uslaner JM (2011) The Selective Phosphodiesterase 9 (PDE9) Inhibitor PF-04447943 Attenuates a scopolamine-induced deficit in a novel rodent attention task. *J Neurogenet* **25**:120-126.

Venkatachalam CM, Jiang X, Oldfield T, and Waldman M (2003) LigandFit: a novel method for the shape-directed rapid docking of ligands to protein active sites. *J Mol Graphics Modell* **21**:289-307.

Verhoest PR, Proulx-Lafrance C, Corman M, Chenard L, Helal CJ, Hou X, Kleiman R, Liu S, Marr E, Menniti FS, Schmidt CJ, Vanase-Frawley M, Schmidt AW, Williams RD, Nelson FR, Fonseca KR, and Liras S (2009) Identification of a brain penetrant PDE9A inhibitor utilizing prospective design and chemical enablement as a rapid lead optimization strategy. *J Med Chem* **52**:7946-7949.

Verhoest PR, Fonseca KR, Hou X, Proulx-LaFrance C, Corman M, Helal CJ, Claffey MM, Tuttle JB, Coffman KJ, Liu S, Nelson F, Kleiman RJ, Menniti FS, Schmidt CJ, Vanase-Frawley M, and Liras S (2012) Design and discovery of 6-[(3S,4S)-4-Methyl-1-(pyrimidin-2-ylmethyl)pyrrolidin-3-yl]-1-(tetrahydro-2H-pyran-4-yl)-1,5-dihydro-4H-pyrazolo[3,4-d]pyrimidin-4-one (PF-04447943), a selective brain penetrant PDE9A inhibitor for the treatment of cognitive disorders. *J Med Chem* **55**:9045-9054.

Wang H, Liu Y, Chen Y, Robinson H, and Ke H (2005) Multiple elements jointly determine inhibitor selectivity of cyclic nucleotide phosphodiesterases 4 and 7. *J Biol Chem* **280**:30949-30955.

Wang H, Liu Y, Huai Q, Cai J, Zoraghi R, Francis SH, Corbin JD, Robinson H, Xin Z, Lin G, and Ke H (2006) Multiple conformations of phosphodiesterase-5: implications for enzyme function and drug development. *J Biol Chem* **281**:21469-21479.

Wang H, Liu Y, Hou J, Zheng M, Robinson H, and Ke H (2007a) Structural insight into substrate specificity of phosphodiesterase 10. *Proc Natl Acad Sci U S A* **104**:5782-5787.

Wang H, Yan Z, Geng J, Kunz S, Seebeck T, and Ke H (2007b) Crystal structure of the Leishmania major phosphodiesterase LmjPDEB1 and insight into the design of the parasite-selective inhibitors. *Mol Microbiol* **66**:1029-1038.

Wang H, Yan Z, Yang S, Cai J, Robinson H, and Ke H (2008a) Kinetic and structural studies of phosphodiesterase-8A and implication on the inhibitor selectivity. *Biochemistry* **47**:12760-12768.

Wang H, Ye M, Robinson H, Francis SH, and Ke H (2008b) Conformational variations of both phosphodiesterase-5 and inhibitors provide the structural basis for the physiological effects of vardenafil and sildenafil. *Mol Pharmacol* **73**:104-110.

Wang H, Luo X, Ye M, Hou J, Robinson H, and Ke H (2010) Insight into binding of phosphodiesterase-9A selective inhibitors by crystal structures and mutagenesis. *J Med Chem* **53**:1726-1731.

Wang H, Kunz S, Chen G, Seebeck T, Wan Y, Robinson H, Martinelli S, and Ke H. (2012) Biological and structural characterization of Trypanosoma cruzi phosphodiesterase C and implications for design of parasite selective inhibitors. *J Biol Chem* **287**:11788-11797.

Winn MD, Murshudov GN, and Papiz MZ (2003) Macromolecular TLS refinement in REFMAC at moderate resolutions. *Methods Enzymol* **374**:300-321.

Wu G, Robertson DH, Brooks CL, III, and Vieth M (2003) Detailed analysis of grid-based molecular docking: A case study of CDOCKER-A CHARMm-based MD docking algorithm. *J Comput Chem* **24**:1549-1562.

Wunder F, Tersteegen A, Rebmann A, Erb C, Fahrig T, and Hendrix M (2005) Characterization of the first potent and selective PDE9 inhibitor using a cGMP reporter cell line. *Mol Pharmacol* **68**:1775-1781.

Footnotes

This work is partially supported by US NIH GM59791 (H.K.), Natural Science Foundation of China [21272287, 81373258] and Major Project of Guangdong Province [2012A080201007], Guangdong Natural Science Foundation [S2011030003190, S2013010014867], Guangzhou Science Foundation [2014J4100165], and the Research Fund for the Doctoral Program of Higher Education of China [20130171110096].

PDB ID Codes

The atomic coordinates and structure factors have been deposited into the RCSB Protein Data Bank with accession codes 4Y86, 4Y87, and 4Y8C.

[#] Manna Huang and Yong-xian Shao contributed equally.

Molecular Pharmacology Fast Forward. Published on August 27, 2015 as DOI: 10.1124/mol.115.099747
This article has not been copyedited and formatted. The final version may differ from this version.

Figure legends

Fig. 1. Chemical structures of PDE9 inhibitors assessed in this study. Symbol * marks a chiral carbon.

Fig. 2. Ribbon diagram of PDE9-**C33**. (A) The PDE9A dimer that has been observed in all PDE9 structures. Inhibitor **C33** is shown as yellow sticks. (B) Superposition of subunit A (cyan, residues 185-506) over B (green).

Fig. 3. Binding of **C33** to PDE9A. (A) Surface presentation on binding of (R)-**C33** (orange sticks) and (S)-**C33** (yellow) to PDE9 dimers. (R)-**C33** and (S)-**C33** showed unique conformation in the PDE9 dimer structures, but in the PDE9 dimer in complex with racemic **C33**, (R)-**C33** binds subunit B and (S)-**C33** binds subunit A. The grey and cyan sticks represent the key residues involved in binding. Dotted lines represent hydrogen bonds. (B) Ribbon model for (S)-**C33** binding to the PDE9 dimer. The red mesh is the electron density in the difference (F_o-F_c) map that was calculated from the structure with omission of (S)-**C33** and contoured at 3σ. (C) Binding of (R)-**C33** to subunit B of the PDE9 dimer.

Fig. 4. The M-pocket for inhibitor binding. (A) Surface model of the M-pocket of PDE9. (B) Superposition of PDE9 (green ribbons) over PDE5 (pale) and PDE8A (salmon). Dotted lines represent hydrogen bonds. (C) Sequence alignment for region around the M-pocket of PDEs. The green color highlights helices in the crystal structures. Two residues in red color gate the pocket.

Fig. 5. The M-pockets in other PDE families. (A) Surface presentation of the M-pocket of PDE5. (B) Surface presentation of the M-pocket of PDE8A. IBMX is a non-selective inhibitor of PDEs. (C) Ribbon presentation of the superposition of PDE9 (green) over PDE1B (cyan). The M-loop of PDE1B is partially disordered. The corresponding residues between PDE9A2 and PDE1B are: M365/M336, N405/H373, L420/L388, L421/M389, Y424/F392, Q453/Q421, and F456/F424.

Molecular Pharmacology Fast Forward. Published on August 27, 2015 as DOI: 10.1124/mol.115.099747
This article has not been copyedited and formatted. The final version may differ from this version.

Table 1. Statistics on diffraction data and structure refinement

Data collection	PDE9-**C33**	PDE9-(S)-**C33**	PDE9-(R)-**C33**
Space group	$P4_12_12$	$P4_12_12$	$P4_12_12$
Unit cell (*a, c*, Å)	103.6, 268.7	104.7, 270.3	105.4, 270.1
Resolution (Å)	2.0	2.7	3.1
Total measurements	1,215,951	688,294	161,116
Unique reflections	96,827	42,348	24,552
Completeness (%)	97.2 (91.9) *	100.0 (100.0)	84.9 (85.4)
Average I/σ	20.8 (3.5) *	7.2 (5.1)	7.6 (2.0)
Rmerge	0.074 (0.274) *	0.125 (0.668)	0.156 (0.717)
Structure Refinement			
R-work	0.224 (0.457)*	0.205(0.291)	0.215 (0.301)
R-free	0.247 (0.470)*	0.231 (0.326)	0.244 (0.364)
Resolution (Å)	30.0-2.0	50.0-2.7	50.0-3.1
Reflections	94,640 (5%) ‡	40,241 (5%)	23,302 (5%)
RMSD for			
bond length (Å)	0.007	0.008	0.007
bond angle (^{o})	1.1	1.1	1.1
Average B-factor (Å^2)			
Protein	40.4 (5357)§	41.6 (5337)	62.1 (5357)
Inhibitor	37.9 (50)	37.8 (50)	61.3 (50)
Zn^{2+}	48.1 (2)	51.7 (2)	71.8 (2)
Mg^{2+}	31.8 (2)	32.5(2)	50.6 (2)
Water	39.0 (255)	29.1 (12)	42.6 (12)
Ramachandran plot (%)			
Favored	93.8	93.0	91.5
Allowed	5.9	6.3	8.3
Generally allowed	0.3	0.7	0.2
Disallowed	0.0	0.0	0.0

*The numbers in parentheses are for the highest resolution shells of 2.0-2.05, 2.7-2.77, and 3.1-3.17 Å, respectively for the PDE9 structures in complex with racemic **C33**, (S)-**C33**, and (R)-**C33**.

‡The percentage of reflections omitted for calculation of R-free.

§The number of atoms in the structure refinement.

Molecular Pharmacology Fast Forward. Published on August 27, 2015 as DOI: 10.1124/mol.115.099747
This article has not been copyedited and formatted. The final version may differ from this version.

Table 2. Inhibition of synthetic compounds on PDE9

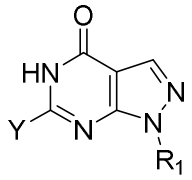

Compounds	Y	R_1	IC_{50} ± SD* (nM)
H10	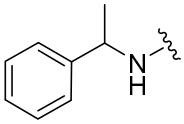		111 ± 14
H35	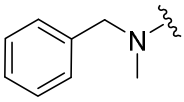		105 ± 35
H33	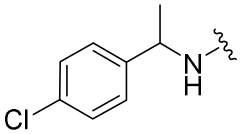		23 ± 5
C10	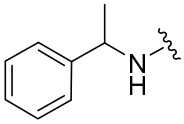	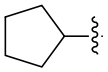	39 ± 15
C35	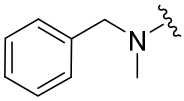	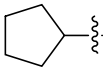	20 ± 2
C33	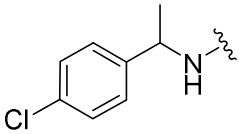	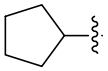	16 ± 4
C40	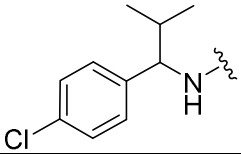	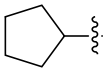	74 ± 5
K10	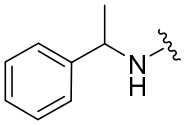	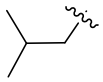	80 ± 15
K35	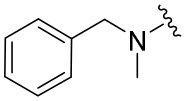	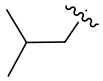	37 ± 4
K33	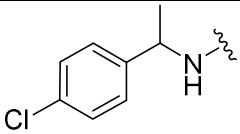	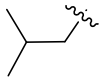	47 ± 8

*Standard deviations were calculated from triply repeated experiments.

Molecular Pharmacology Fast Forward. Published on August 27, 2015 as DOI: 10.1124/mol.115.099747
This article has not been copyedited and formatted. The final version may differ from this version.

Table 3. Affinity of **C33** with PDE families (IC_{50}, nM)

PDEs	(S)-**C33**	**C33**	(R)-**C33**	**3r** §
PDE9A (181-506)	11 ± 4	16 ± 4	58 ± 2	0.60±0.02
PDE1B2 (10-487)	554 ± 64 (46)*	152 ± 15 (9)	80±4 (1.4)	473 ± 14 (800)
PDE2A3 (222-904)	2.4 ± 0.5 x10^3 (200)	437 ± 77 (27)	479±79 (8)	13 ± 0.2 x10^3 (22000)
PDE4D2 (86-413)	1.3 ± 0.1 x10^3 (108)	1.8 ± 0.2 x10^3 (110)	3.2 ± 0.6 x10^3 (56)	21 ± 0.7 x10^3 (35000)
PDE5A1 (535-860)	366 ± 38 (31)	197 ± 36 (12)	787 ± 38 (14)	91 ± 23 (151)
PDE7A1 (130-482)	2.5 ± 0.4 x10^3 (208)	1.7 ± 0.1 x10^3 (104)	1.3 ± 0.1 x10^3 (23)	1.8 ± 0.7 x10^3 (3000)
PDE8A1 (480-820)	1.0 ± 0.2 x10^3 (83)	1.6 ± 0.2 x10^3 (98)	4.4 ± 0.4 x10^3 (76)	>100,000
PDE10A2 (448-789)	2.3 ± 0.3 x10^3 (192)	1.2 ± 0.1 x10^3 (73)	774 ± 11 (13)	6.9 ± 0.1 x10^3 (11000)

*The numbers in parentheses are the fold of selectivity of inhibitors against PDE9 over other PDEs.

§ The data are cited from the paper by Shao et al., 2014.

Molecular Pharmacology Fast Forward. Published on August 27, 2015 as DOI: 10.1124/mol.115.099747
This article has not been copyedited and formatted. The final version may differ from this version.

Table 4. Pharmacokinetics profile of PDE9 inhibitor **C33**

Dosing Route	$T_{1/2}$ (h)	T_{max}(h)	C_{max} (ng/ml)	AUC_{0-t} ng.h/mL	AUC_{0-inf} ng.h/mL	MRT_{inf} (h)	Vz (L/kg)	CLz (L/h/kg)	F (%)
PO	1.5 ± 0.2	2.0 ± 0.0	372 ± 6	1600±300	1700±300	3.5 ± 0.3	NA	NA	56.5
IV	1.4 ± 0.1	0.02 ± 0.00	5300 ± 900	3000±200	3100±200	1.6 ± 0.2	3.2 ± 0.1	1.6 ± 0.1	

PO = oral administration

IV = Intravenous administration

Molecular Pharmacology Fast Forward. Published on August 27, 2015 as DOI: 10.1124/mol.115.099747
This article has not been copyedited and formatted. The final version may differ from this version.

Table 5A**.** Metabolic stability of PDE9 inhibitors in human liver microsome

Compound	k	$T_{1/2}$ (min)	Cl_{int} (mL/min/mg)	Cl_{app} (mL/min/mg)	Cl_h (mL/min/mg)	E_h (%)
Testosterone	0.035	20.0	0.069	66.9	15.4	78.0
Warfarin	-0.001	stable	stable	stable	stable	
(S)-**C33**	0.007	105	0.013	12.7	7.8	38.9
(R)-**C33**	0.016	44.0	0.032	30.4	12.1	60.3
Racemic **C33**	0.013	51.4	0.027	26.0	11.3	56.5
C40	0.011	62.2	0.022	21.5	10.4	51.8
3r*	0.058	11.9	0.116	112	17.0	84.8

*The data are cited from paper by Shao et al., 2014.

Table 5B. Metabolic stability of PDE9 inhibitors in mouse liver microsome

Compound	k	$T_{1/2}$ (min)	Cl_{int} (mL/min/mg)	Cl_{app} (mL/min/mg)	Cl_h (mL/min/mg)	E_h (%)
Testosterone	0.165	4.2	0.329	1296	84.2	93.5
Warfarin	-0.003	stable	stable	stable	stable	
(S)-**C33**	0.013	53.5	0.026	102	47.8	53.1
(R)-**C33**	0.034	20.2	0.069	270	67.5	75.0
Racemic **C33**	0.022	31.3	0.044	174	59.4	66.0
C40	0.002	291	0.008	19	15.5	17.2
3r*	0.031	22.3	0.062	244	65.8	73.1

*The data are cited from paper by Shao et al., 2014.

Molecular Pharmacology Fast Forward. Published on August 27, 2015 as DOI: 10.1124/mol.115.099747
This article has not been copyedited and formatted. The final version may differ from this version.

Table 6. The average difference between Cα atoms of subunits A and B of the PDE9 dimers (Å)

	C33	4QGE (**3r**)	4GH6 (**28s**)	3JSI	3JSW	4G2J	4G2L	3K3E	3QI3	2HD1	3DYN (cGMP)	3DY8 (GMP)
residues 181-506	0.32	0.33	0.36	0.32	0.35	0.33	0.31	0.41	0.43	0.39	0.31	0.30
M-loop (S433-K446)	0.59	0.65	0.58	0.48	0.74	0.74	0.67	1.11	1.34	0.80	0.92	0.70

Figure 1

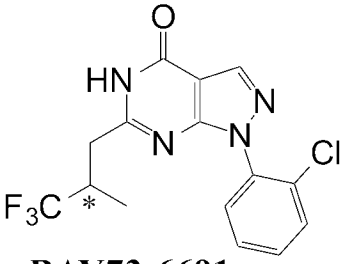

BAY73-6691

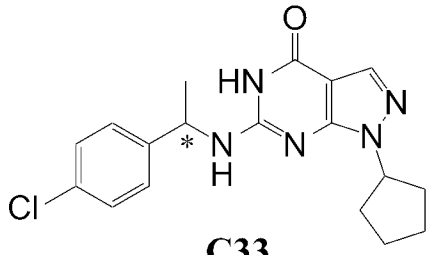

C33

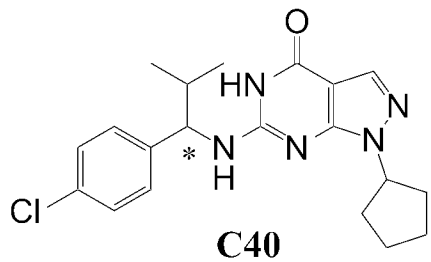

C40

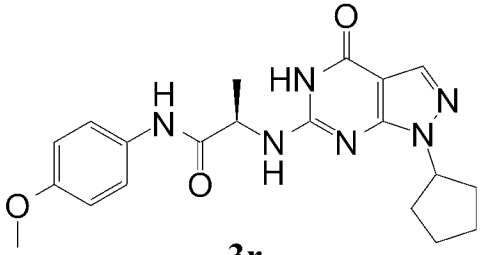

3r

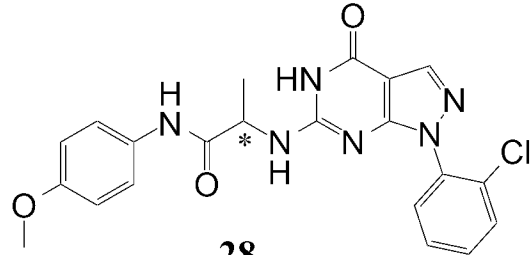

28

Figure 2

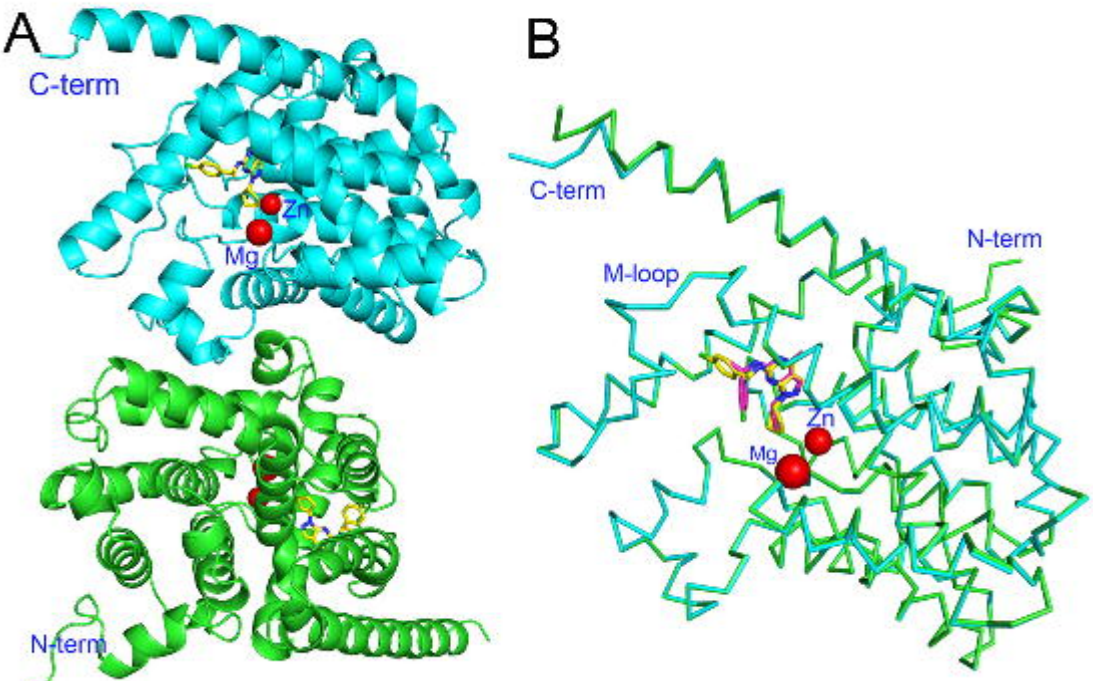

Figure 3

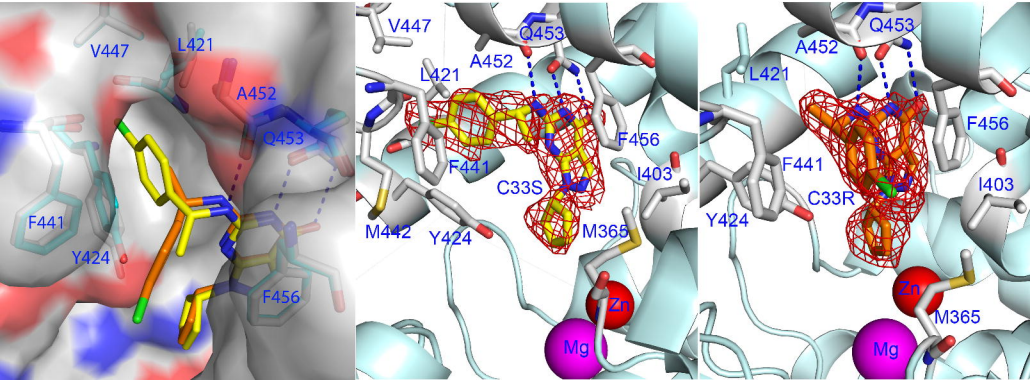
V447
L421
A452
Q453
F441
Y424
F456
V447
Q453
A452
L421
F456
F441
C33S
I403
M442
Y424
M365
Zn
Mg
Q453
A452
L421
F456
F441
C33R
I403
Y424
Zn
M365
Mg

Figure 4

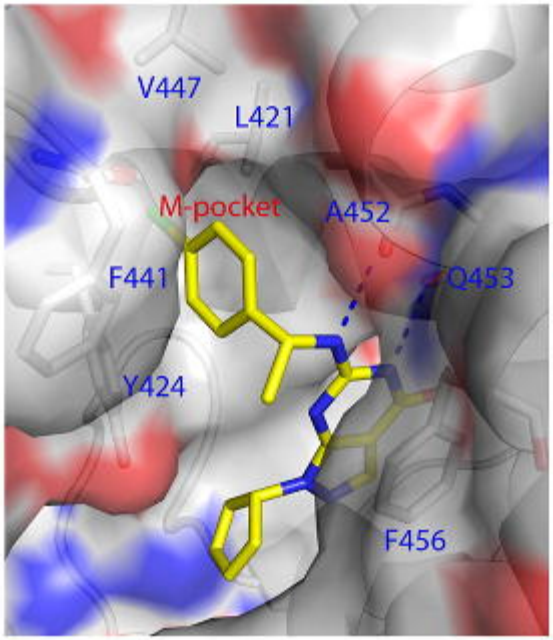

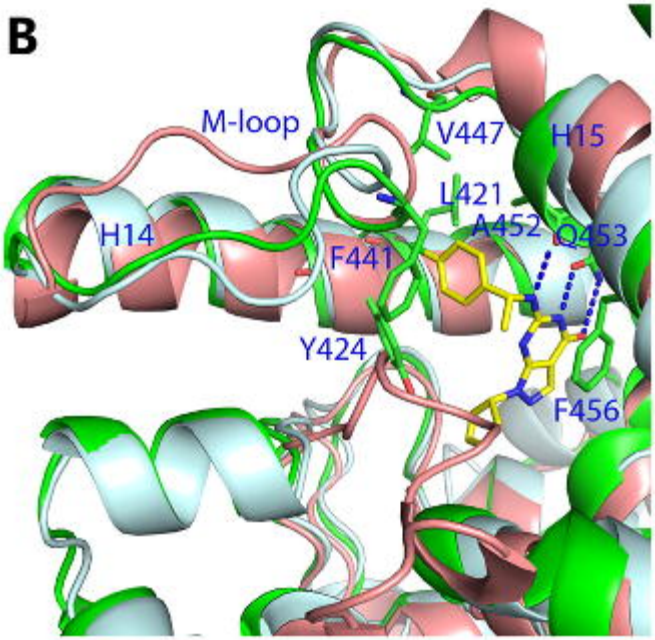

C

```
                    H14                          |←   M-loop   →|  H15
PDE9A2   MEVAEPWV DCLLEEYFMQSDREK SEGLPVA--PFMDRD -KVTKATAQIGFIKFV 460
PDE1B1   WLVHSRWT KALMEEFFRQGDKEA ELGLPFS--PLCDRT -STLVAQSQIGFIDFI 427
PDE5A1   WPIQQRIA ELVATEFFDQGDRER KELNIEPTD-LMNRE KKNKIPSMQVGFIDAI 824
PDE6C    WEVQSQVA LMVANEFWEQGDLER TVLQQQPIPMMDRNK -RDELPKLQVGFIDFV 782
PDE4D2   LQLYRQWT DRIMEEFFRQGDRER ERGMEIS--PMCDKH -NASVEKSQVGFIDYI 376
PDE8A1   LQYCIEWA ARISEEYFSQTDEEK QQGLPVVM-PVFDRN -TCSIPKSQISFIDYF 784
PDE7A1   WELSKQWS EKVTEEFFHQGDIEK KYHLGVS--PLCDRH -TESIANIQIGFMTYL 419
PDE2A3   WKTTRKIA ELIYKEFFSQGDLEK AMGNRPM--EMMDRE -KAYIPELQISFMEHI 865
PDE3B    RDLHLKWT EGIVNEFYEQGDEEA NLGLPIS--PFMDRS -SPQLAKLQESFITHI 994
PDE10A2  WPVTKLTA NDIYAEFWAEGDEMK KLGIQPI--PMMDRD KKDEVPQGQLGFYNAV 732
PDE11A2  WEISRQVA ELVTSEFFEQGDRER LELKLTPS-AIFDRN RKDELPRLQLEWIDSI 625
tcrPDEC1 GVAIARKW LVILQEFADQAEDER RRGLPVT--PGFETP --SSVEKSQIPFLDFF 577
tbrPDEB1 PFDISRQW MAVTEEFYRQGDMEK ERGVEVL--PMFDRS KNMELAKGQIGFIDFV 881
lmjPDEB1 PFETSRMW MAVTEEFYRQGDMEK EKGVEVL--PMFDRS KNNELARGQIGFIDFV 894
```

Figure 5

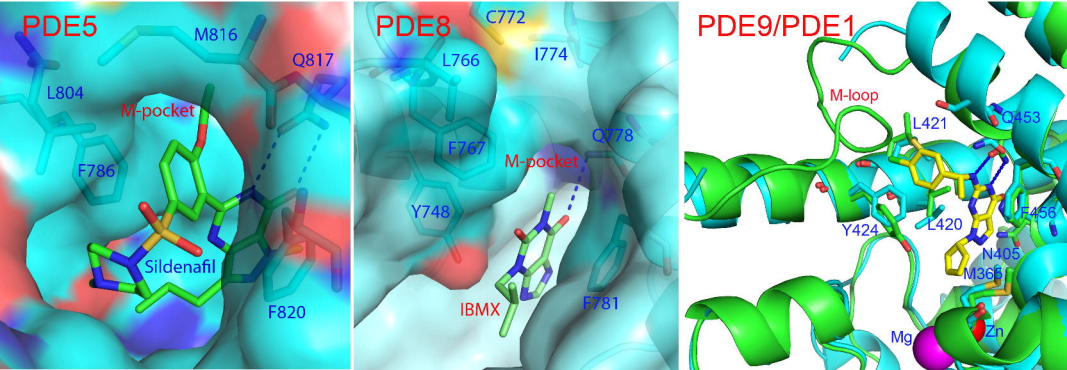
PDE5
M816
Q817
L804
M-pocket
F786
Sildenafil
F820
PDE8
C772
L766
I774
F767
Q778
M-pocket
Y748
IBMX
F781
PDE9/PDE1
M-loop
L421
Q453
F456
Y424
L420
N405
M365
Mg
Zn